PCCP

PAPER

View Article Online
View Journal | View Issue

Cite this: *Phys. Chem. Chem. Phys.*, 2018, **20**, 13340

Asymmetric twins in boron rich boron carbide

Xiaokun Yang,[a] William A. Goddard III [b] and Qi An *[ac]

Received 4th March 2018,
Accepted 12th April 2018

DOI: 10.1039/c8cp01429a

rsc.li/pccp

Twin boundaries (TBs) play an essential role in enhancing the mechanical, electronic and transport properties of polycrystalline materials. However, the mechanisms are not well understood. In particular, we considered that they may play an important role in boron rich boron carbide ($B_{vr}BC$), which exhibits promising properties such as low density, super hardness, high abrasion resistance, and excellent neutron absorption. Here, we apply first-principles-based simulations to identify the atomic structures of TBs in $B_{vr}BC$ and their roles for the inelastic response to applied stresses. In addition to symmetric TBs in $B_{vr}BC$, we identified a new type of asymmetric twin that constitutes the phase boundaries between boron rich boron carbide ($B_{13}C_2$) and $B_{vr}BC$ ($B_{14}C$). The predicted mechanical response of these asymmetric twins indicates a significant reduction of the ideal shear strength compared to single crystals $B_{13}C_2$ and $B_{14}C$, suggesting that the asymmetric twins facilitate the disintegration of icosahedral clusters under applied stress, which in turn leads to amorphous band formation and brittle failure. These results provide a mechanistic basis towards understating the roles of TBs in $B_{vr}BC$ and related superhard ceramics.

1. Introduction

Twin boundaries (TBs), separating two crystals through a mirror plane, are formed during the processes of crystal growth, annealing and deformation[1,2] and are ubiquitous in many crystalline solids. In contrast to traditional grain boundaries (GBs), which are incoherent, TBs generally exhibit small lattice mismatch so that they are energetically more stable. Consequently, TBs significantly affect the mechanical, electronic and transport properties of realistic materials.[3–5] In particular, the formation of nanoscale twins can significantly affect the plasticity and strength of metals and ceramics. For example, nanotwinned Cu is ten times stronger than coarse-grained Cu.[4] Another example is that nanotwins in ceramics have been found to dramatically enhance the strength and hardness of diamond and boron nitride.[6,7]

TBs can be identified easily in relatively simple systems such as FCC, BCC, and HCP metals. However, they become quite complex for more complicated crystal structures that exhibit secondary and tertiary structural hierarchies. For example, Fujita *et al.*[8] used high-resolution transmission electron microscopy (HRTEM) to discover a new type of TB in carbon rich boron carbide (B_4C) where the angle between the (100) and (010) rhombohedral planes differs by $\sim 2^\circ$ on either side of the TBs. This type of TB is referred to as an "asymmetric twin" because of the loss of twin symmetry. Our further study combining HRTEM and first-principles-based simulations indicated that this "asymmetric twin" in B_4C is associated with the distribution of carbon atoms into various positions within the 12-atom icosahedron.[9]

Boron carbides have been widely used as high performance ceramic materials where hardness and weight are critical because of their promising properties such as low density, ultra-high hardness, good thermal stability, and low material costs.[10–14] They are also of great interest for nuclear applications because of their high neutron absorption and self-healing capacities.[15] Similar to other ceramics and metal alloys, the mechanical properties of boron carbides depend strongly on the chemical composition, microstructure, and fabrication processes.[14,16–20] Boron carbides, consisting of a 12-atom icosahedron with a 3-atom chain in a rhombohedral unit, possess very complex crystalline structures. They have a wide composition range of 8.8–20 at% C.[14,16,20,21] Beyond $\sim$20 at% C, a mixture of B_4C and graphite is often observed. Below $\sim$8 at% C, α-boron usually co-exists with B_4C.[20,22] Only two stoichiometries have been proposed as candidates for stable boron carbides:

(1) B_4C with the configuration $(B_{11}C_p)$CBC where the icosahedral carbon is located at a polar site that connects directly to other icosahedra;[13]

(2) the boron rich boron carbide ($B_{13}C_2$) with the atomic configuration (B_{12})CBC.[23]

The atomic structures in the regime below $\sim$13.3 at% C (or $B_{vr}BC$) have not previously been identified, but it was proposed that they may be the combination of B_{12}, $B_{11}C$, $B_{10}C_2$, and B_9C_3 icosahedra and CCC, CBC, CCB, CBB, BCB, and BBB chains.

[a] *Department of Chemical and Materials Engineering, University of Nevada, Reno, Reno, Nevada, 89577, USA. E-mail: qia@unr.edu*
[b] *Materials and Process Simulation Center, California Institute of Technology, Pasadena, California 91125, USA*
[c] *Nevada Institute for Sustainability, University of Nevada, Reno, Reno, Nevada 89557, USA*

Previous studies[24] have shown that high density twins can be introduced experimentally into B_4C, $B_{13}C_2$ and $B_{vr}BC$.[16] Close examinations of these materials showed that both symmetric twins and "asymmetric twins" are present in highly twinned samples of B_4C and $B_{vr}BC$.[8,16] Previous study suggests that asymmetric twins in B_4C are formed because the C atoms can be distributed in polar sites (connected to icosahedra) or equatorial sites (connected to CBC chains) within the ($B_{11}C$) icosahedron.[9] As the B content increases to $B_{13}C_2$, only symmetric twins can be observed because the icosahedral carbon is replaced by B atoms to form the (B_{12}) icosahedron.[9,23] Recently, Cheng *et al.* observed the growth of two types of twins in $B_{vr}BC$ samples ($B_{7.8}C$ and $B_{10.2}C$) using HRTEM. One type of twin is the conventional symmetric twin with a twin angle of $72.8 \pm 0.2^\circ$.[16] This type of twin agrees well with our QM predicted twins in $B_{13}C_2$ in which (B_{12})CBC configurations are on both sides of TBs.[9] However, most twins in the $B_{vr}BC$ samples are "asymmetric twins" with twin angles of $72.8 \pm 0.2^\circ$ and $74.1 \pm 0.2^\circ$ on two sides of TBs.[16] It was speculated that the increased population of asymmetric twins could be associated with the monoclinic distortion of the structure caused by excess boron atoms.[16] However, the atomic structures and formation mechanisms have not been explained. Previous study only examined the crystal structures for $B_{14}C$ but provides no information on the possible twinned structures in $B_{vr}BC$.[25] Clearly the formation of "asymmetric twins" must be related directly to the hierarchical levels of $B_{vr}BC$ structures. We recently investigated the deformation mechanisms of symmetric twins in $B_{13}C_2$ and found that these nanotwins significantly decreased the strength of single crystal $B_{13}C_2$.[23] This is in contrast with the nanotwins in B_4C where the nanotwins increased the strength of single crystal B_4C.[24] However, it remains unclear how the nanotwins affect the mechanical properties of $B_{vr}BC$.

In the present study, we first apply first-principles-based simulations (density functional theory (DFT) at the Perdew–Burke–Ernzerhof (PBE) level) to demonstrate that the "asymmetric twins" in $B_{vr}BC$ are actually the phase boundaries of (B_{12})CBC and (B_{12})CBB. Particularly, in the (B_{12})CBB phase, the C–B–B chain can be either a kinked chain or a linear chain, as discussed in our previous study.[25] Then we examined the response of these asymmetric twins to applied stress and derived the stress–strain relationships, the ideal shear strength, and the failure mechanisms. We find that the asymmetric twins lead to a lower ideal shear strength than those of both (B_{12})CBC and (B_{12})CBB, suggesting a softening effect. However, under the stress conditions appropriate for an indentation experiment, we find that the asymmetric twins lead to a higher critical stress than that of (B_{12})CBB, but lower than that of (B_{12})CBC. The failure mechanism for asymmetric twins arises from the interaction between the icosahedral clusters and the C–B–B chains under pure shear deformation. However, under indentation the failure initiates from the interactions of both C–B–B and C–B–C chains with their nearest icosahedra.

2. Computational methodology

All the DFT calculations were performed with the VASP package,[26–28] using the PBE functional and the projector augmented wave (PAW) method to account for the core–valence interactions.[29] The electron partial occupancies were determined using the tetrahedron method with Blöchl corrections. The energy cutoff for the plane wave expansion was 600 eV. Brillouin zone integration was performed on Γ-centered symmetry-reduced Monkhorst–Pack meshes with a fine resolution of $2\pi \times 1/40$ Å^{-1} for all calculations except for the shear deformation. The energy error for terminating the electronic self-consistent field (SCF) and the force criterion for the geometry optimization were set equal to 10^{-6} eV and 10^{-3} eV Å^{-1}, respectively.

To determine the ideal shear strength for the asymmetric twinned structure, we applied the pure shear deformation along the TBs by imposing the shear strain along the twin plane while allowing full structural relaxation for the other five strain components.[30] To simulate the mechanical response under indentation experiments, we applied biaxial shear deformation on the asymmetric twined structure. This simulation aims at mimicking deformation under the indenter by imposing the relation $\sigma_{zz} = \sigma_{zx} \times \tan \Phi$, where σ_{zz} is the normal stress, σ_{zx} is the shear stress and Φ is the centerline-to-face angle of the indenter ($\Phi = 68^\circ$ for Vickers indenter).[7] The other four strain components are relaxed in biaxial shear deformations. The residual stresses after relaxing were less than 0.5 GPa for both pure shear and biaxial shear deformations. A more approximate $2 \times 2 \times 2$ k-point grid mesh in the Brillouin zone was applied in both pure shear and biaxial shear deformations. Since the shear strain is constrained in the deformation, the stress of the system may become negative after the structure changes or fails.

3. Results and discussion

To characterize the asymmetric twins in $B_{vr}BC$, two boron carbide configurations were considered: (B_{12})CBC and (B_{12})CBB. Fig. 1(a) displays the (B_{12})CBC crystal structure ($2 \times 1 \times 4$ supercell) with the $R\bar{3}m$ space group, where the B_{12} icosahedral cluster is located on the corner and the C–B–C chain is along the [111] rhombohedral directions. Here, crystal planes and directions are given using a 3-index rhombohedral notation. The angle between (100) and (010) was measured to be $\alpha = 73.24^\circ$ in the (B_{12})CBC crystal, as shown in Fig. 1(a).

For the (B_{12})CBB crystal, two atomic structures were considered: the bent C–B–B chain (B_{12})bCBB and the linear C–B–B chain (B_{12})lCBB. Our previous study indicated that (B_{12})bCBB is more stable than (B_{12})lCBB by 0.3 eV per unit cell because it has one 3c-2e bond and two 2c-2e bonds instead of three 3c-2e bonds per unit cell, making (B_{12})bCBB more favorable.[25] The crystalline structure ($2 \times 1 \times 4$ supercell) for (B_{12})bCBB is displayed in Fig. 1(b) with the measured angle $\alpha' = 71.80^\circ$. In contrast, the crystalline structure ($2 \times 1 \times 4$ supercell) for (B_{12})lCBB is displayed in Fig. 1(d) with the measured angle $\alpha' = 73.70^\circ$.

To determine the atomic structures of asymmetric twins, we constructed twinned models with the {100} plane as the TB; here two layers of (B_{12})CBC are on one side and two layers of either (B_{12})bCBB or (B_{12})lCBB structures are on the other side.

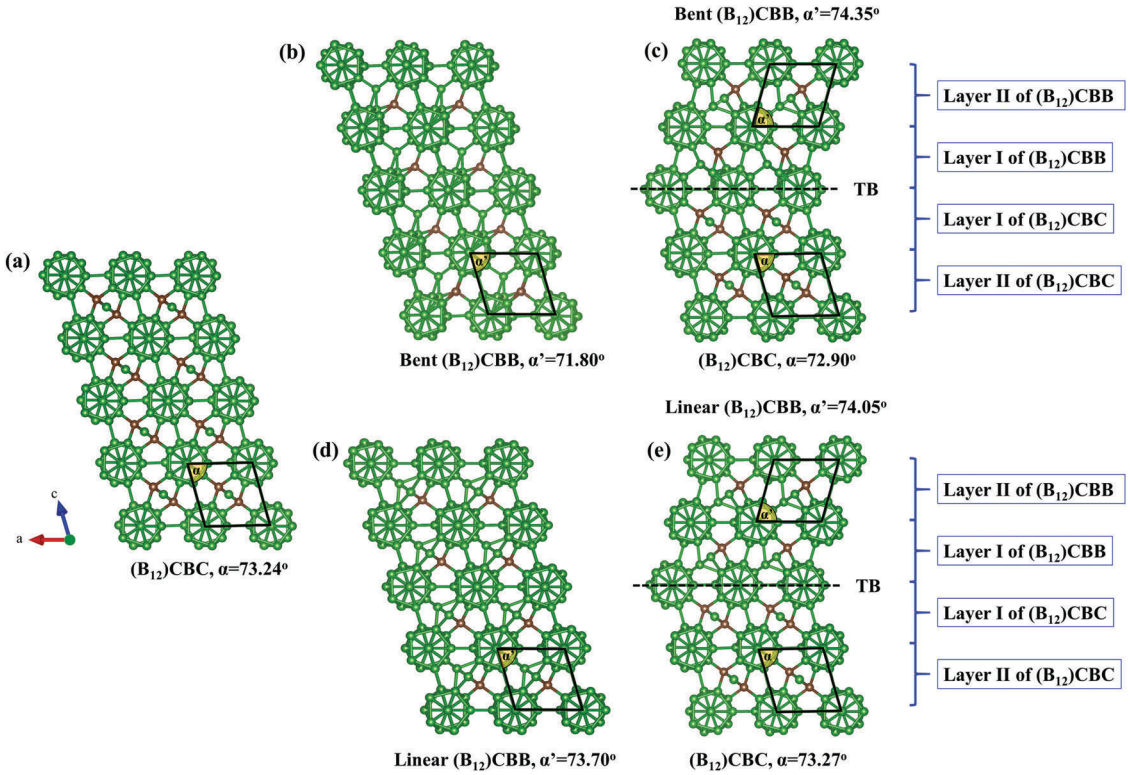

Fig. 1 The atomic models from the DFT simulations: (a) single crystal (B_{12})CBC, (b) single crystal $(B_{12})b$CBB, (c) (B_{12})CBC–$(B_{12})b$CBB asymmetric twin, (d) single crystal $(B_{12})l$CBB, and (e) (B_{12})CBC–$(B_{12})l$CBB asymmetric twin. The TB plane is represented by a dashed black line. The boron and carbon atoms are represented by green and sienna balls, respectively.

We named the 1st nearest layer to the middle TB on the (B_{12})CBB side the layer I of (B_{12})CBB, and named the other layer the layer II of (B_{12})CBB (Fig. 1(c) and (e)). Similarly, on the (B_{12})CBC side, the 1st nearest layer to the middle TB is the layer I of (B_{12})CBC, and the other layer is the layer II of (B_{12})CBC (Fig. 1(c) and (e)).

The twinned model with $(B_{12})b$CBB and (B_{12})CBC contains 120 atoms and was relaxed by DFT simulations, leading to the cell parameters of a = 10.339 Å, b = 5.170 Å, c = 18.087 Å, α = 90.8°, β = 89.2°, and γ = 113.4° with a density of 2.456 g cm^{-3}. The C–B–B chains in layer II become almost linear with a C–B–B angle of 176.7°, while the C–B–B chains in layer I remain bent with a C–B–B angle of 94.3°, as shown in Fig. 1(c). Therefore, the middle TB connects (B_{12})CBC and $(B_{12})b$CBB, while the other edge TB connects (B_{12})CBC and $(B_{12})l$CBB. This is because the lattice mismatch between (B_{12})CBC and $(B_{12})b$CBB is larger than the lattice mismatch between (B_{12})CBC and $(B_{12})l$CBB. This turns one layer of $(B_{12})b$CBB to $(B_{12})l$CBB in this twinned model. The inclination angles were measured to be α = 72.90° and α' = 74.35°, as shown in Fig. 1(c), which agree very well with the experimental measurements of α = 72.8 ± 0.2° and α' = 74.1 ± 0.2°.[16]

Our results suggest that the asymmetric twins observed experimentally[16] are actually the phase boundary of two phases of (B_{12})CBC and (B_{12})CBB. Therefore, the new asymmetric twins are associated with the distribution of boron atoms into various positions within the 3-atom chain and chain deformation (bent *vs.* linear), which is different from the asymmetric twins in B_4C[9] where they are associated with the distribution of carbon atoms in the icosahedron. Our QM simulations predict the interfacial energy of asymmetric twins in $B_{vr}BC$ to be 108.4 mJ m^{-2}, which is higher than that of asymmetric twins in B_4C (83.2 mJ m^{-2})[9] and much higher than that of symmetric twins in $B_{13}C_2$ (40.6 mJ m^{-2}).[23] This higher interfacial energy can be ascribed to the lattice mismatch caused by the kinked C–B–B chain.

In order to examine how the linear C–B–B chain affects the twinned structures, a twinned model with $(B_{12})l$CBB (Fig. 1(e)) was constructed and relaxed *via* DFT simulations, leading to the cell parameters of a = 10.335 Å, b = 5.167 Å, c = 18.130 Å, α = 90.6°, β = 90.6°, and γ = 113.7° with a density of 2.456 g cm^{-3}. The inclination angles were measured to be α = 73.27° and α' = 74.05°. The angle difference is ~0.8°, which is slightly lower than the experimental measurement of 1.3°.[16] The interfacial energy for this twinned model is predicted to be 7.0 mJ m^{-2} if the referent structures are (B_{12})CBC and $(B_{12})l$CBB. Although the small lattice mismatch between (B_{12})CBC and $(B_{12})l$CBB leads to a much lower interfacial energy, this model is 0.1 eV per unit-cell higher in energy than the above twinned model mixing $(B_{12})b$CBB and (B_{12})CBC, suggesting that the above model is the most plausible asymmetric twins under experimental conditions. Therefore, we will focus on the (B_{12})CBC–$(B_{12})b$CBB twinned model when examining the mechanical properties. We will also examine the (B_{12})CBC–$(B_{12})l$CBB twinned model for comparison.

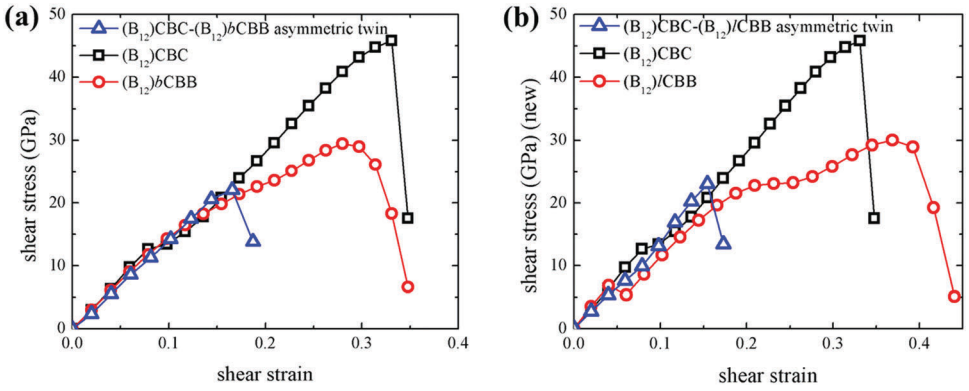

Fig. 2 Shear-stress–shear-strain relationship under pure-shear deformation of (a) the (B_{12})CBC–$(B_{12})b$CBB asymmetric twin (blue △), the single crystal (B_{12})CBC (black □), and the single crystal $(B_{12})b$CBB (red ○), and (b) the (B_{12})CBC–$(B_{12})l$CBB asymmetric twin (blue △), the single crystal (B_{12})CBC (black □), and the single crystal $(B_{12})l$CBB (red ○).

In order to understand the mechanical response of asymmetric twins we applied pure shear deformation on the twinned (B_{12})CBC–$(B_{12})b$CBB model and compared with the single crystals (B_{12})CBC and $(B_{12})b$CBB. Previous experimental studies[11] and our previous QM calculations[31] suggest that the most plausible slip system for B_4C is the (001)[100]. Considering the structure similarity, we sheared the single crystals (B_{12})CBC and $(B_{12})b$CBB along the (001)[100] slip system and sheared the twinned model along the TBs, which corresponds to the {001} plane. The shear-stress–shear-strain relationships for crystalline (B_{12})CBC, $(B_{12})b$CBB and twinned (B_{12})CBC–$(B_{12})b$CBB structures are displayed in Fig. 2(a). The ideal shear strength for the asymmetric twinned model is 22.1 GPa, which is 23.7 GPa and 7.9 GPa lower than those for the single crystals (B_{12})CBC (45.8 GPa) and $(B_{12})b$CBB (30.0 GPa), respectively. Thus, the presence of the nanoscale twins significantly reduces the ideal shear strength of the single crystals (B_{12})CBC and $(B_{12})b$CBB. This suggests that the mechanical failure likely initiates at the asymmetric TB regions in $B_{vr}BC$.

In order to understand how the linear C–B–B chain affects the failure of the asymmetric twinned model, we applied pure shear deformation on the twinned (B_{12})CBC–$(B_{12})l$CBB model and compared to (B_{12})CBC and $(B_{12})l$CBB. The shear-stress–shear-strain relationships for the single crystal (B_{12})CBC, $(B_{12})l$CBB and twinned (B_{12})CBC–$(B_{12})l$CBB models are displayed in Fig. 2(b). The ideal shear strength for the twinned (B_{12})CBC–$(B_{12})l$CBB model is 23.0 GPa, which is much lower than those for single crystals (B_{12})CBC (45.8 GPa) and $(B_{12})l$CBB (30.0 GPa). It is slightly higher than that of the twinned (B_{12})CBC–$(B_{12})b$CBB model although the twinned (B_{12})CBC–$(B_{12})b$CBB model is slightly lower in energy. The failure mechanisms of these two structures will be compared and discussed in the following paragraphs.

Our previous studies concluded that the brittle fracture in B_4C arises from the shear-induced cracking of $(B_{11}C)$, which subsequently leads to an amorphous band region, which then induces cavitation and eventually crack opening.[31,32] To understand how the "asymmetric twins" affect the brittle failure process in $B_{vr}BC$, we examined the detailed structural changes under pure shear deformation.

In the (B_{12})CBC–$(B_{12})b$CBB asymmetric twin, the structure experiences elastic deformation as the shear strain increases from 0 to 0.166. In the two layers of the "asymmetric twins" model, only C–B–B chains in layer I are bent while the C–B–B chains in layer II remaining approximately linear. As the shear strain increases to 0.166, the linear chains in layer II (C6–B43–B107) are deformed from 176.7° to 107.0°, as shown in Fig. 3(b). Meanwhile, the B1–B13 bond within the icosahedron is stretched from 1.820 Å to 1.899 Å. As the shear strain increases further to 0.187 (Fig. 3(c)), the B1–B13 bond breaks with the bond distance increasing to 2.703 Å. Meanwhile, the C6 in the C–B–B chain is bonded to B1 within the icosahedron (bond distance is 1.803 Å). This leads to the deconstruction of the icosahedra, releasing the shear stress from 22.1 GPa to 13.8 GPa. The failure arises from the interaction between the (B_{12}) icosahedra and the C–B–B chains in layer II while the chains in layer I remain intact. During the whole failure process, the structure in the (B_{12})CBC region does not disintegrate. This is consistent with our prediction that the ideal shear strength of (B_{12})CBC is much higher than that of (B_{12})CBB.

Detailed structural changes of the (B_{12})CBC–$(B_{12})l$CBB asymmetric twin under pure shear deformation are analyzed and shown in Fig. 4. The linear C–B–B chains in both layers are bent when the shear strain is applied. The angle of C6–B43–B107 in layer II of the (B_{12})CBB region bends from 176.7° to 116.0° at 0.155 strain, causing the middle B43 in the C–B–B chain to approach the nearest icosahedron (1.883 Å). The C9–B108–B98 angle in layer I of the (B_{12})CBB region also bends, as shown in Fig. 4(b), similarly to the (B_{12})CBC–$(B_{12})b$CBB twin. Meanwhile, the B1–B13 bond within the icosahedron is stretched from 1.803 to 1.827 Å. As the shear strain further increases to 0.173 (Fig. 4(c)), the B1–B13 bond breaks with the bond distance increasing to 2.755 Å, and the chain atom C6 is bonded to the cage atom B1 with a bond distance of 1.805 Å. This leads to the deconstruction of the icosahedra, releasing the shear stress from 23.0 GPa to 13.4 GPa. In the layer I region, B98 and B108 atoms slightly adjust their positions leading to the bent C–B–B chain angle of 101.8°. Similar to (B_{12})CBC–$(B_{12})b$CBB, the brittle failure of the (B_{12})CBC–$(B_{12})l$CBB asymmetric twin also arises

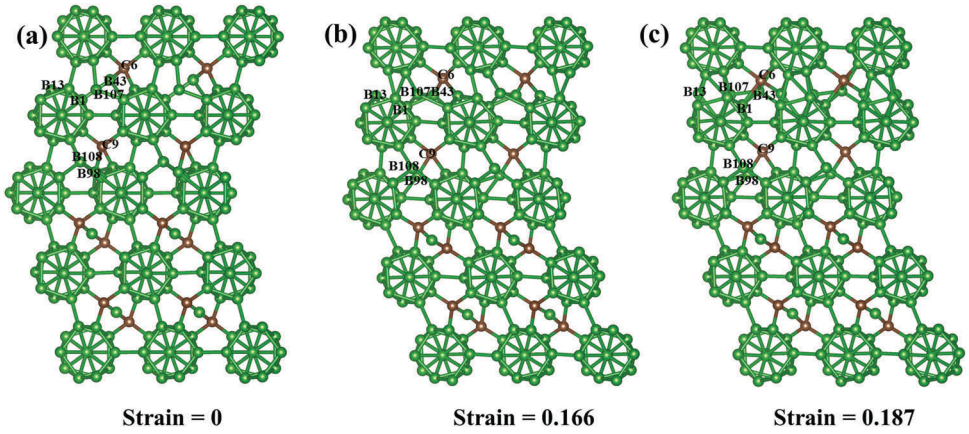

Fig. 3 Structure evolution of (B_{12})CBC–(B_{12})*b*CBB asymmetric twin under pure shear deformation: (a) intact structure; (b) the structure at 0.166 strain before failure, the B–B bond within the icosahedra is stretched in layer II of (B_{12})CBB and (c) the failed structure at 0.187 strain.

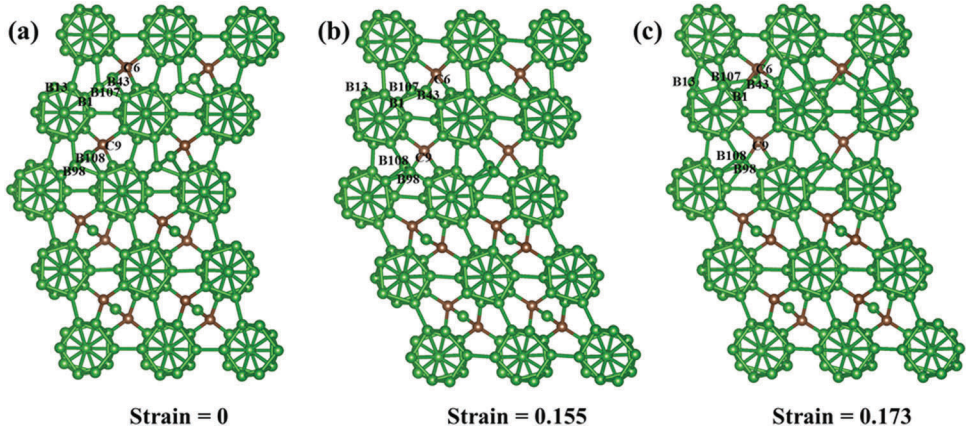

Fig. 4 Structure evolution of (B_{12})CBC–(B_{12})*l*CBB asymmetric twin under pure shear deformation: (a) intact structure; (b) the structure at 0.155 strain before failure, the B–B bond within the icosahedra is stretched in the upper half (B_{12})CBB region; and (c) the failed structure at 0.173 strain.

from the interaction between the (B_{12}) icosahedra and the C–B–B chains in the layer II of the (B_{12})CBB region.

Our previous study[23] showed that the brittle failure in (B_{12})CBC arises from the direct disintegration of icosahedra, which leads to a higher ideal shear strength. This suggests that (B_{12})CBC is stronger than $B_{vr}BC$. Therefore, it is essential to decrease the B content to improve the strength of boron carbide. The failure process of the asymmetric twinned structure is similar to that of crystalline (B_{12})*b*CBB[25] where the B1–B13 bond breaks, leading to the deconstruction of the icosahedra.

We suggest that micro- and nanoindentation experiments could be carried out to validate our predicted strength of asymmetric twinned structures, crystalline (B_{12})CBC and (B_{12})CBB. However, the stress conditions under indentation experiments are very complex compared to our simulated pure shear deformation. To predict material behaviors under indentation experiments, we performed biaxial shear deformation to mimic the stress conditions under indentation.[7] The shear-stress–shear-strain relationships for the asymmetric twinned structures, single crystal (B_{12})CBC and single crystal (B_{12})CBB are shown in Fig. 5. The (B_{12})CBC–(B_{12})*b*CBB asymmetric twin has a maximum shear stress of 22.3 GPa, which is 22.0% lower than that of single crystal (B_{12})CBC (28.6 GPa). However, it is higher than that of single crystal (B_{12})*b*CBB (20.8 GPa). For the (B_{12})CBC–(B_{12})*l*CBB asymmetric twin, the maximum shear stress is 26.5 GPa, which is 4.2 GPa and 5.7 GPa higher than that of the (B_{12})CBC–(B_{12})*b*CBB asymmetric twin and single crystal (B_{12})*l*CBB, respectively, but it is lower than that of single crystal (B_{12})CBC. These results indicate that the hardness of the (B_{12})CBC–(B_{12})*l*CBB asymmetric twin should be higher than that of the single crystalline (B_{12})*l*CBB but lower than that of the single crystal (B_{12})CBC.

The detailed deformation processes of the (B_{12})CBC–(B_{12})*b*CBB asymmetric twin under biaxial shear conditions are displayed in Fig. 6. Since a compressive stress is applied, the upper (B_{12})CBB and lower (B_{12})CBC regions experience different failure processes. As the shear strain increases to 0.187, the C6–B43–B107 chain in layer II of the (B_{12})CBB region bends to 154.4° (shown in Fig. 6(b)). A slight stress release is observed as the shear strain increases from 0.187 to 0.209. By examining the detailed structural change, we find that the C–B–B chain in layer I of the (B_{12})CBB region bends from 117.2° to 100.0° by adjusting the position of B98 and B108 atoms.

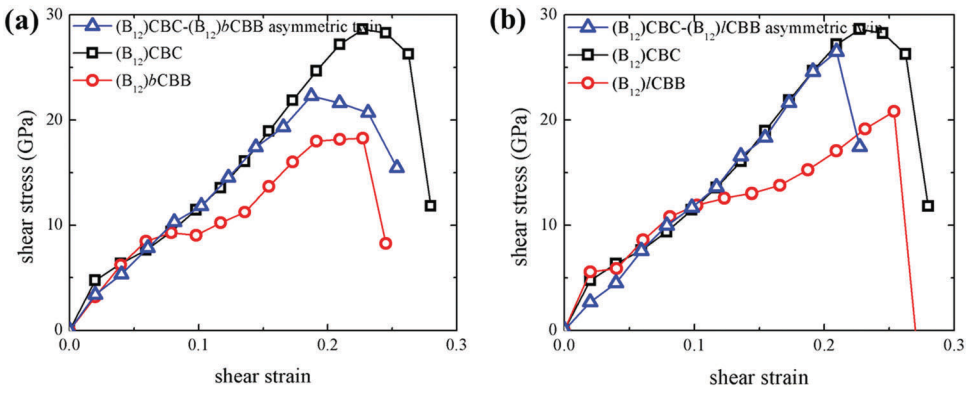

Fig. 5 Shear-stress–shear-strain relationship under biaxial shear conditions of (a) the (B_{12})CBC–(B_{12})*b*CBB asymmetric twin (blue △), the single crystal (B_{12})CBC (black □), and the single crystal (B_{12})*b*CBB (red ○), and (b) (B_{12})CBC–(B_{12})*l*CBB asymmetric twin (blue △), the single crystal (B_{12})CBC (black □), and the single crystal (B_{12})*l*CBB (red ○).

As the shear strain further increases to 0.254, the adjusted chain atom B108 bonds with B63 from icosahedra in layer I of the (B_{12})CBB region. Therefore, the icosahedra in layer I of the (B_{12})CBB region are deconstructed (shown in Fig. 6(d)) by breaking the icosahedral B63–B68 bond. Meanwhile, the icosahedra in the TB region are deformed as well because of the highly compressive stress. A new B68–B33 bond is formed, connecting two adjacent icosahedra in (B_{12})CBB and TB regions. Interestingly, when the twinned structure is deconstructed, the C6–B43–B107 chain in layer II of the (B_{12})CBB region turns back to 172.6°.

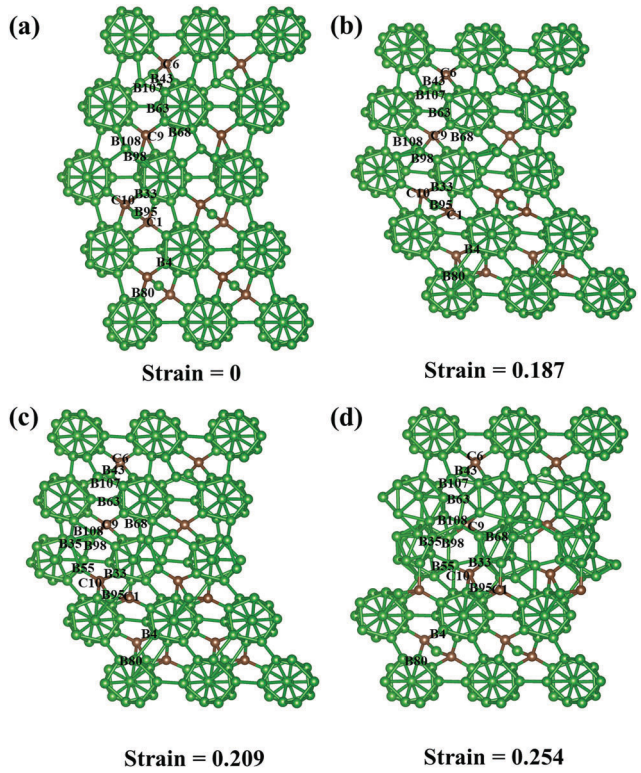

Fig. 6 Structure evolution of the (B_{12})CBC–(B_{12})*b*CBB twin under biaxial shear deformation: (a) intact structure; (b) the structure at 0.187 strain before failure, both C–B–B and C–B–C chains in layer II bend; (c) the structure at 0.209 strain before failure; and (d) the failed structure at 0.245 strain.

Different from pure shear conditions, under biaxial shear conditions, the structure in the (B_{12})CBC region is deformed, but not destroyed. However, the (B_{12})CBB region is deconstructed. The originally linear C10–B95–C1 chain in layer I of the (B_{12})CBC region continuously bends when the shear strain increases. The B4–B80 bond in the layer II of the (B_{12})CBC region initially forms at 0.187 strain and then breaks at 0.254 strain. The icosahedra in the (B_{12})CBC region are not deconstructed, but the C10 atom from the bent C–B–C chain in layer I of the (B_{12})CBC region bonds to B55, causing the B35–B55 icosahedral bond breaking within the TB region, thus contributing to the full deconstruction of the twinned structure.

Therefore, under biaxial shear conditions, the (B_{12})CBC–(B_{12})*b*CBB asymmetric twin fails in both layer I of the (B_{12})CBB region and the TB regions because of three main factors: (1) the interaction between the C–B–B chain and icosahedra in layer I of the (B_{12})CBB region; (2) the interaction between the C–B–C chain and icosahedra in layer I of the (B_{12})CBC region; and (3) the highly compressive stress conditions.

The detailed deformation processes of the (B_{12})CBC–(B_{12})*l*CBB asymmetric twin under biaxial shear deformation are displayed in Fig. 7. As the shear strain increases to 0.209, all C–B–B and C–B–C chains bent slightly without any bond breaking as shown in Fig. 7(b). However, the icosahedra in both (B_{12})CBB and (B_{12})CBC regions are deformed while the TB region remains intact as the shear strain further increases to 0.227 (shown in Fig. 7(c)). In the (B_{12})CBB region, icosahedra in both layer I and layer II are deconstructed by pressing the B51 in layer II down and forming a new B51–B107 bond with the C–B–B chain. Meanwhile, the C9 from the C–B–B chain in layer I forms a new bond to B68 from the icosahedra of layer I in the (B_{12})CBB region, causing the B68–B56 icosahedral bond to break, which leads to the deconstruction of the whole (B_{12})CBB region. In the (B_{12})CBC region, the layer II icosahedra are also deconstructed at 0.277 strain by the interaction between the C8–B42–C5 chain and the icosahedra, as shown in Fig. 7(c).

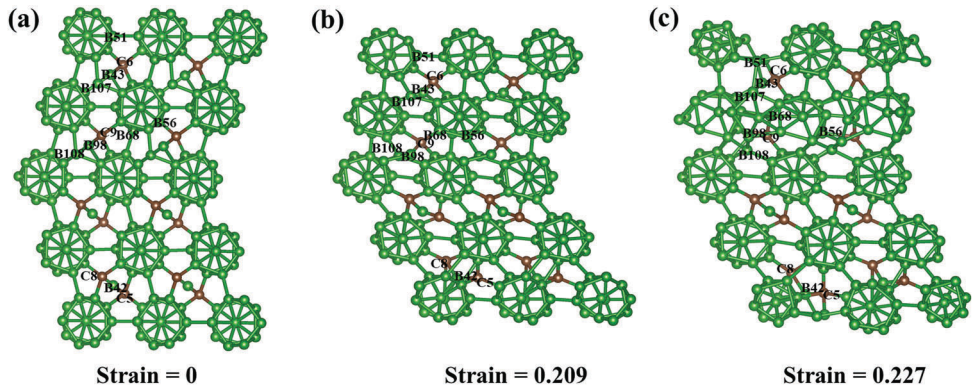

Fig. 7 Structure evolution of the $(B_{12})CBC–(B_{12})lCBB$ asymmetric twin under biaxial shear deformation: (a) intact structure; (b) structure at 0.209 strain before failure; and (c) failed structure at 0.227 strain.

4. Conclusion

In summary, we used first-principles-based simulations to identify a new type of "asymmetric twins" in $B_{vr}BC$. The new "asymmetric twins" are actually a phase boundary of two configurations of $(B_{12})CBC$ and $(B_{12})CBB$. We also compared the linear and bent C–B–B chain effects in the asymmetric twinned structure. We then examined the deformation and failure mechanisms of these "asymmetric twins" in $B_{vr}BC$ under both pure shear and biaxial shear conditions. The major findings include:

• Under pure shear deformation the asymmetric twinned structures have a lower ideal shear strength than those of single crystals $(B_{12})CBC$ and $(B_{12})CBB$, suggesting that the amorphous shear bands prefer to initiate at these weak planar defects in $B_{vr}BC$. The failure mechanism for asymmetric twinned structures involves the interaction of the C–B–B chains with the icosahedral clusters at the TBs.

• Under biaxial shear conditions, the ideal shear strength of the asymmetric twins is higher than that of single crystal $(B_{12})CBB$, but lower than that of single crystal $(B_{12})CBC$. This arises from the different failure mechanisms under indentation loading conditions. Particularly, the icosahedra in $(B_{12})CBB$ and TB regions are deconstructed by the interaction between both C–B–B and C–B–C chains and the icosahedra in $(B_{12})CBB$ and TB regions in the $(B_{12})CBC–(B_{12})bCBB$ twin. However, the icosahedra in both $(B_{12})CBB$ and $(B_{12})CBC$ regions are deconstructed yet the icosahedra in the TB region remains intact in the $(B_{12})CBC–(B_{12})lCBB$ asymmetric twin because of the interactions of both C–B–B and C–B–C chains with icosahedra in the layer II regions.

Summarizing our studies on nanotwins in boron carbides, the asymmetric twin in B_4C is actually the phase boundary of the ground state structure $(B_{11}C_p)CBC$ and high energy structure of $(B_{11}C_e)CBC$. However, the asymmetric twin in $B_{vr}BC$ is the phase boundary of $(B_{12})CBC$ and $(B_{12})CBB$ in which the CBB chain can be linear or kink. Only symmetric twin can be observed in $B_{13}C_2$ because of the relatively simple configuration of $(B_{12})CBC$. Nanotwins can strengthen B_4C, even exceed the ideal shear strength, but they can impair the strength of $B_{13}C_2$ and $B_{vr}BC$ structures.

Conflicts of interest

There are no conflicts to declare.

Acknowledgements

This work was supported by the National Science Foundation (CMMI–1727428, program manager, Siddiq Qidwai).

References

1 Q. Yu, L. Qi, K. Chen, R. K. Mishra, J. Li and A. M. Minor, The nanostructured origin of deformation twinning, *Nano Lett.*, 2012, **12**, 887–892.
2 K. Lu, L. Lu and S. Suresh, Strengthening materials by engineering coherent internal boundaries at the nanoscale, *Science*, 2009, **324**, 349–352.
3 A. Nie, L. Y. Gan, Y. Cheng, Q. Li, Y. Yuan, F. Mashayek, H. Wang, R. Klie, U. Schwingenschlogl and R. Shahbazian Yassar, Twin Boundary-Assisted Lithium Ion Transport, *Nano Lett.*, 2015, **15**, 610–615.
4 L. Lu, X. Chen, X. Huang and K. Lu, Revealing the maximum strength in nanotwinned copper, *Science*, 2009, **323**, 607–610.
5 K. C. Kim, J. Lee, B. K. Kim, W. Y. Choi, H. J. Chang, S. O. Won, B. Kwon, S. K. Kim, D. Bin Hyun, H. J. Kim, H. C. Koo, J. H. Choi, D. I. Kim, J. S. Kim and S. H. Baek, Free-electron creation at the 60° twin boundary in Bi_2Te_3, *Nat. Commun.*, 2016, **7**, 12449.
6 Y. Tian, B. Xu, D. Yu, Y. Ma, Y. Wang, Y. Jiang, W. Hu, C. Tang, Y. Gao, K. Luo, Z. Zhao, L. M. Wang, B. Wen, J. He and Z. Liu, Ultrahard nanotwinned cubic boron nitride, *Nature*, 2013, **493**, 385–388.
7 B. Li, H. Sun and C. Chen, Large indentation strain-stiffening in nanotwinned cubic boron nitride, *Nat. Commun.*, 2014, **5**, 4965.
8 T. Fujita, P. Guan, K. M. Reddy, A. Hirata, J. Guo and M. Chen, Asymmetric twins in rhombohedral boron carbide, *Appl. Phys. Lett.*, 2014, **104**, 21907.
9 K. Y. Xie, Q. An, M. F. Toksoy, J. W. McCauley, R. A. Haber, W. A. Goddard III and K. J. Hemker, Atomic-Level Understanding

of 'asymmetric Twins' in Boron Carbide, *Phys. Rev. Lett.*, 2015, **115**, 175501.
10 M. W. Chen, J. W. McCauley and K. J. Hemker, Shock-Induced Localized Amorphization in Boron Carbide, *Science*, 2003, **299**, 1563–1566.
11 K. M. Reddy, P. Liu, A. Hirata, T. Fujita and M. W. Chen, Atomic structure of amorphous shear bands in boron carbide, *Nat. Commun.*, 2013, **4**, 2483.
12 N. Vast, J. Sjakste and E. Betranhandy, Boron carbides from first principles, *J. Phys.: Conf. Ser.*, 2009, **176**, 12002.
13 V. Domnich, S. Reynaud, R. A. Haber and M. Chhowalla, Boron carbide: structure, properties, and stability under stress, *J. Am. Ceram. Soc.*, 2011, **94**, 3605–3628.
14 F. Thevenot, Boron carbide-A comprehensive review, *J. Eur. Ceram. Soc.*, 1990, **6**, 205–225.
15 D. Simeone, C. Mallet, P. Dubuisson, G. Baldinozzi, C. Gervais and J. Maquet, Study of boron carbide evolution under neutron irradiation by Raman spectroscopy, *J. Nucl. Mater.*, 2000, **277**, 1–10.
16 C. Cheng, K. M. Reddy, A. Hirata, T. Fujita and M. W. Chen, Structure and mechanical properties of boron-rich boron carbides, *J. Eur. Ceram. Soc.*, 2017, **37**, 4514–4523.
17 K. Y. Xie, K. Livi, J. W. McCauley and K. J. Hemker, Precipitation of AlN in a commercial hot-pressed boron carbide, *Scr. Mater.*, 2015, **101**, 95–98.
18 J. E. Saal, S. Shang, Z. K. Liu, J. E. Saal, S. Shang and Z. Liu, The structural evolution of boron carbide via ab initio calculations The structural evolution of boron carbide via ab initio calculations, *Appl. Phys. Lett.*, 2007, **91**, 231915.
19 M. W. Chen, J. W. McCauley, J. C. LaSalvia and K. J. Hemker, Microstructural characterization of commercial hot-pressed boron carbide ceramics, *J. Am. Ceram. Soc.*, 2005, **88**, 1935–1942.
20 M. Bouchacourt and F. Thevenot, The properties and structure of the boron carbide phase, *J. Less-Common Met.*, 1981, **82**, 227–235.
21 D. Gosset and M. Colin, Boron carbides of various compositions: an improved method for X-rays characterisation, *J. Nucl. Mater.*, 1991, **183**, 161–173.
22 M. Beauvy, Stoichiometric limits of carbon-rich boron carbide phases, *J. Less-Common Met.*, 1983, **90**, 169–175.
23 Q. An and W. A. Goddard III, Nanotwins soften boron-rich boron carbide ($B_{13}C_2$), *Appl. Phys. Lett.*, 2017, **110**, 111902.
24 Q. An, W. A. Goddard III, K. Y. Xie, G. D. Sim, K. J. Hemker, T. Munhollon, M. Fatih Toksoy and R. A. Haber, Superstrength through Nanotwinning, *Nano Lett.*, 2016, **16**, 7573–7579.
25 X. Yang, W. A. Goddard III and Q. An, Structure and Properties of Boron-Very-Rich Boron Carbides: B_{12} Icosahedra Linked through Bent CBB Chains, *J. Phys. Chem. C*, 2018, **122**, 2448–2453.
26 G. Kresse and J. Hafner, *Ab initio* molecular dynamics for liquid metals, *Phys. Rev. B: Condens. Matter Mater. Phys.*, 1993, **47**, 558–561.
27 G. Kresse and J. Furthmüller, Efficient iterative schemes for ab initio total-energy calculations using a plane-wave basis set, *Phys. Rev. B: Condens. Matter Mater. Phys.*, 1996, **54**, 11169–11186.
28 G. Kresse and J. Furthmüller, Efficiency of *ab initio* total energy calculations for metals and semiconductors using a plane-wave basis set, *Comput. Mater. Sci.*, 1996, **6**, 15–50.
29 G. Kresse, From ultrasoft pseudopotentials to the projector augmented-wave method, *Phys. Rev. B: Condens. Matter Mater. Phys.*, 1999, **59**, 1758–1775.
30 D. Roundy, C. Krenn, M. Cohen and J. Morris, Ideal Shear Strengths of fcc Aluminum and Copper, *Phys. Rev. Lett.*, 1999, **82**, 2713–2716.
31 Q. An, W. A. Goddard III and T. Cheng, Atomistic Explanation of Shear-Induced Amorphous Band Formation in Boron Carbide, *Phys. Rev. Lett.*, 2014, **113**, 95501.
32 Q. An and W. A. Goddard III, Atomistic Origin of Brittle Failure of Boron Carbide from Large-Scale Reactive Dynamics Simulations: Suggestions toward Improved Ductility, *Phys. Rev. Lett.*, 2015, **115**, 105501.